ACADEMIC PRESS

Available online at www.sciencedirect.com

SCIENCE DIRECT®

Journal of Sound and Vibration 265 (2003) 1047–1061

JOURNAL OF SOUND AND VIBRATION

www.elsevier.com/locate/jsvi

Sinusoidal reference strategy for adaptive feedforward vibration control: numerical simulation and experimental study

F.J. Peng[a,*], M. Gu[a], H.-J. Niemann[b]

[a] *Department of Bridge Engineering, Tongji University, Shanghai 200092, People's Republic of China*
[b] *Boundary Layer Wind Tunnel Laboratory, Ruhr-Universität Bochum, D-44780 Bochum, Germany*

Received 4 July 2001; accepted 21 August 2002

Abstract

A new control approach named Sinusoidal Reference Strategy is developed for adaptive feedforward structural control. In this approach, the recursive-least-squares algorithm is used and a higher frequency sinusoidal signal is utilized as the reference signal. The present approach is able to overcome some of the shortcomings of the conventional adaptive feedforward control. Numerical simulations are then conducted on reducing wind-induced vibrations of the JIN MAO Building in Shanghai, China, with a height of 420 m. A multiple-degree-of-freedom (m.d.o.f.) aeroelastic model of a general super-tall building and an active mass damper (AMD) actuator are designed and manufactured. Wind tunnel tests are carried out to investigate further the control efficiency and robustness of the present approach. Both the simulation and experimental results show that the approach can reduce vibration of super-tall buildings remarkably, and can adapt to dynamic uncertainties and modelling errors of the buildings.

1. Introduction

Nowadays, more and more super-tall buildings are being constructed worldwide. These kinds of structures are sensitive to wind excitations due to their low damping and stiffness, and thus large amplitude vibrations often occur under strong wind excitation. For serviceability considerations, it is important to develop some effective approaches to reduce the vibration level of such kind of buildings. Active structural control has turned out to be an effective means to

*Corresponding author. Directorate of Spacecraft Engineering, Canadian Space Agency, 6767 Route de L'Aeroport, Saint-Hubert, QC, Canada J3Y 8Y9. Tel.: +1-450-926-6683.
E-mail address: fujun.peng@space.gc.ca (F.J. Peng).

0022-460X/03/$ - see front matter
doi:10.1016/S0022-460X(02)01600-0

reduce wind-induced response, and a number of control algorithms have been developed [1–7], most of which are generally based on an accurate model of the structure to be controlled. However, for super-tall buildings under wind excitation, damping and stiffness are varying with time due to the aerodynamic effects, and thus their dynamic properties are difficult to model accurately. The characteristics of wind-induced vibrations of super-tall buildings thus impose a new and stricter requirement for the robustness of control algorithms. One promising control methodology is the adaptive feedforward control algorithm, which does not require an accurate model of the structure, and can tolerate changes of structural dynamic properties. The adaptive feedforward control algorithm stemmed from adaptive signal processing and was first applied in the 1970s to the cancellation of signals corrupted by noise or interference [8,9]. In the 1980s, it was implemented for the active control of acoustics [10]. Then it was extended to the control of radiated sound from harmonically excited structures [11], as well as broadband structural vibration [12]. More recently, this technique has been applied to vibration control of civil engineering structures [13,14]. In the previous studies, the reference signal for the adaptive feedforward control was assumed to be available directly from the excitation source in most cases. A sinusoidal signal or multiple harmonic signal was also used as the reference signal, mostly for controlling a sinusoidal response or harmonic response. However, wind excitations are of high uncertainty with respect to magnitude and arrival time, and the original excitations are difficult to be picked up and used as the reference signal for adaptive feedforward control. Thus, the construction of a reference signal becomes one of the critical issues for adaptive feedforward control of wind-induced vibration of super-tall buildings. In this paper, a Sinusoidal Reference Strategy is developed and some properties of the control system are discussed. Numerical simulations are conducted on reducing wind-induced vibration of the JIN MAO building. A multiple-degree-of-freedom (m.d.o.f.) aeroelastic model of a general super-tall building and an active mass damper (AMD) are designed and manufactured. Wind tunnel tests are performed on controlling the along-wind and the across-wind vibrations of the building model, respectively. Both the simulation and experimental results demonstrate high control efficiencies and good robustness of the strategy.

2. Principle of conventional adaptive feedforward control

The block diagram of the conventional adaptive feedforward control is shown in Fig. 1, where, $\mathbf{P}_1$ is the transfer property of the controlled structure from the external excitation to the sensor; $\mathbf{P}_2$ is the transfer property from the control force to the sensor; $\mathbf{H}$ is the N-order identified finite impulse response (FIR) model of $\mathbf{P}_2$; $\mathbf{W}$ is a FIR controller; $\boldsymbol{x}$ is the reference signal; $\boldsymbol{f}$ is the external excitation; $\boldsymbol{d}$ is the response to the external excitation; $\boldsymbol{u}$ is the control force; $\boldsymbol{s}$ is the response to the control force; $\boldsymbol{e}$ is the error response, i.e., the sum of the responses to external excitation and control force. The adaptive algorithm adjusts controller parameters in real time according to the error responses measured by sensors, and makes these parameters converge to their optimal values.

There are broadly three key issues for the conventional adaptive feedforward control: (1) Construction of the reference signal. The basic requirement of it is to be correlated with the external excitations or the uncontrolled response. (2) Determination of orders of the FIR model

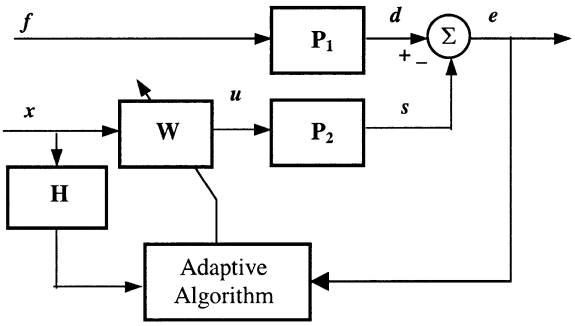

Fig. 1. Block diagram of adaptive feedforward control.

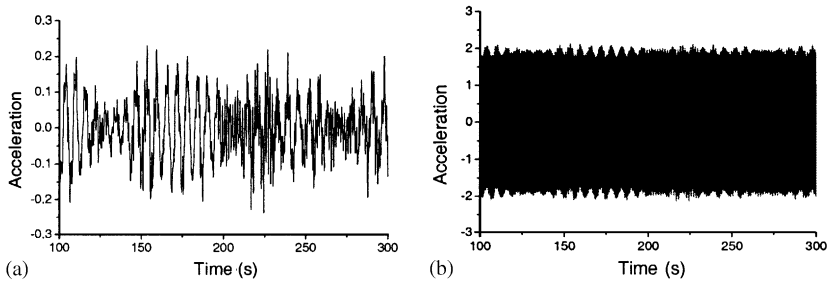

Fig. 2. A sample of typical uncontrolled response and mixed response; (a) original uncontrolled response, (b) mixed response.

and controller. They are normally determined based on the number of frequency components in the reference signal (or the frequency bandwidth of the reference signal). More components correspond to large sizes. (3) Development of the adaptive algorithm. There are two broad classes of adaptive algorithms that can be used for adaptive feedforward control [15–17]. One is the least-mean-squares (LMS) algorithm and the other is the recursive-least-squares (RLS) algorithm. The former has been widely used for its simplicity in computation (with a complexity of $O(N)$, where N denotes the order of the FIR model), but its property is limited because of its slow convergence rate. The latter has superior convergence property and tracking capability, but its complicated computation (with a complexity of $O(N^2)$) may become an obstacle in some practical applications, especially in multi-channel cases.

3. Development of sinusoidal reference strategy

From the vibration cancellation point of view, one of the difficulties in reducing wind-induced vibration of super-tall buildings comes from the violent variation of the uncontrolled response, a typical sample of which is shown in Fig. 2(a). As a solution, a higher frequency sinusoidal signal is added here to the original uncontrolled response and the mixed response is regarded as the objective response to be controlled. The mixed response is shown in Fig. 2(b). Considering the

relatively alleviated variation of the amplitude, one can expect intuitively that better results may be obtained than controlling the original response directly.

The mixed response is dominated by the additional sinusoidal signal; therefore, the reference signal for adaptive feedforward control can be determined as a sinusoidal signal with the same frequency. Then the block diagram of the adaptive feedforward control system evolves into Fig. 3, where K is a proportional coefficient, used for adjusting the amplitude of the additional sinusoidal signal. In order to improve tracking capability of the control system, a filtered-x RLS algorithm is used here. Define the N-order FIR model of the control path H, the N-order FIR controller $W(n)$ as

$$\mathbf{H} = [h_1 h_2 \cdots h_N], \tag{1}$$

$$\mathbf{W}(n) = [w_1 w_2 \cdots w_N]. \tag{2}$$

The corresponding recursive algorithm can be expressed as

$$x(n) = A \sin(n\omega\,\Delta t), \tag{3}$$

$$\mathbf{X}_N(n) = [x(n)x(n-1)\cdots x(n-N+1)], \tag{4}$$

$$y(n) = \mathbf{X}_N(n)\mathbf{H}^{\mathrm{T}}, \tag{5}$$

$$\mathbf{Y}_N(n) = [y(n)y(n-1)\cdots y(n-N+1)], \tag{6}$$

$$\mathbf{P}_N(n) = \mathbf{C}_{NN}(n-1)\mathbf{Y}_N^{\mathrm{T}}(n), \tag{7}$$

$$\mu = \mathbf{Y}_N(n)\mathbf{P}_N(n), \tag{8}$$

$$\mathbf{g}_N(n) = \mathbf{P}_N(n)/(\lambda + \mu), \tag{9}$$

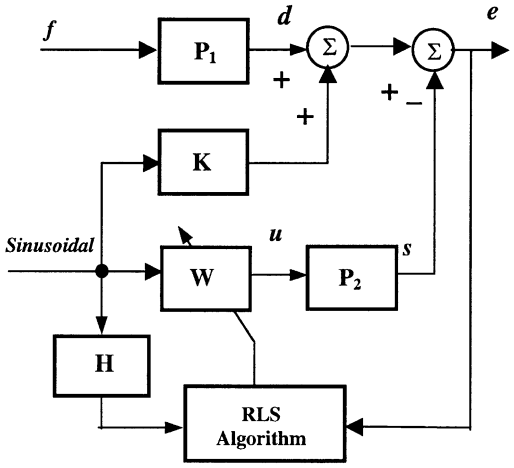

Fig. 3. Block diagram of adaptive feedforward control for reducing mixed response.

$$\mathbf{C}_{NN}(n) = \frac{1}{\lambda}\left[\mathbf{C}_{NN}(n-1) - \frac{\mathbf{P}_N(n)\mathbf{P}_N^{\mathrm{T}}(n)}{(\lambda+\mu)}\right], \tag{10}$$

$$\mathbf{W}(n) = \mathbf{W}(n-1) + \mathbf{g}_N^{\mathrm{T}}(n)e(n), \tag{11}$$

$$u(n) = \mathbf{X}_N(n)\mathbf{W}^{\mathrm{T}}(n), \tag{12}$$

where $x(n)$ is the present time value of the reference signal, n is the time index, λ is the forgetting factor of the adaptive algorithm, Δt is the time interval of control update, A and ω are the amplitude and the circular frequency of the reference signal, respectively, $e(n)$ is the error response which is the sum of uncontrolled response, the added sinusoidal and the secondary response produced by control signal; $u(n)$ is the control signal at present time. After obtaining the FIR model $\mathbf{H}$ and initializing the FIR controller $\mathbf{W}$, one can obtain the controller coefficients and control signal at every time index by using Eqs. (3)–(12) iteratively.

In the control system shown in Fig. 3, the control signal u consists of two components: one corresponds to the uncontrolled response and the other corresponds to the additional sinusoidal signal. The former is the desired component for reducing the original uncontrolled response. But the latter will lead to additional undesired response if it is applied to the structure directly. In order to remove this negative effect, Eq. (11) is investigated in more detail. It can be re-written as

$$\mathbf{W}_1(n) + \mathbf{W}_2(n) = \mathbf{W}_1(n-1) + \mathbf{W}_2(n-1) + \mathbf{g}_N^{\mathrm{T}}(n)(e_1(n) + e_2(n)), \tag{13}$$

where $\mathbf{W}_1(n)$ and $\mathbf{W}_2(n)$ are two components of the controller corresponding to the two control signal components respectively. $e_1(n)$ and $e_2(n)$ are error components corresponding to the original uncontrolled response and the additional signal.

When $\mathbf{W}_2(n)$ converges sufficiently, $\mathbf{W}_2(n)$ is approximately identical to $\mathbf{W}_2(n-1)$, and $e_2(n)$ is much less than $e_1(n)$ and thus can be neglected in Eq. (13). So one can have

$$\mathbf{W}_1(n) = \mathbf{W}_1(n-1) + \mathbf{g}_N^{\mathrm{T}}(n)e_1(n). \tag{14}$$

Eq. (14) shows that the recursive computation of $\mathbf{W}_1(n)$ is separated from the value of $\mathbf{W}_2(n)$ as well as the amplitude of the additional sinusoidal signal. Therefore, the proportional coefficient K in Fig. 3 is set as zero, thus $\mathbf{W}_2(n)$ becomes definitely a zero vector. So the negative influence of the addition is removed and the control signal contains only the desired component. The block diagram of the SRS-based adaptive feedforward control is shown in Fig. 4.

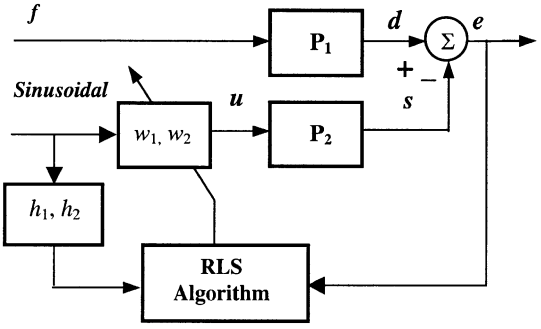

Fig. 4. Block diagram of SRS-based adaptive feedforward control.

It seems that Fig. 4 is very similar to the conventional adaptive feedforward control. But in fact it has some unique characteristics: (1) Its reference signal is definitely selected as a sinusoid, whose frequency is much higher than all of the dominant modal frequencies of the controlled structure. This is quite different from the conventional principle for selecting a reference signal. (2) The orders of the FIR model and the controller are definitely selected as 2, since the reference signal is only of a 2-order persistent excitation. Theoretically, this is the smallest size for them. Such a small size can remarkably reduce the computation amount during each control update interval, and thus make the algorithm more easy to implement. (3) Identification of the FIR model is conducted offline using an adaptive identification method with the same sinusoid as input signal. The updating rate is selected as the same as that for controlling. Only the dominant modes are included through using modal filters. Such a modelling method means that the two parameters of the FIR model only reflects amplitude and phase properties at a high-frequency point. It is well known that a vibration system appears to be nearly inertial under high-frequency excitations, and amplitude and phase properties are not sensitive to the fluctuation of damping and stiffness of the vibrating system. The present modelling method, therefore, is helpful to improve the robustness of the whole control system. It should be noted that the same modal filters should be used for both identification and control.

4. Numerical simulation

The SRS-based adaptive feedforward control is simulated for reducing wind-induced vibrations of the JIN MAO Building, 420 m high, located in Pudong New Area, Shanghai, China. Only the first three modes are considered. Their mode shapes and modal frequencies are shown in Fig. 5 and Table 1, respectively. The terrain condition is considered as category D. The exponent α of the average wind profile is 0.3 and the corresponding gradient height is 450 m according to Chinese code. The 10-year return period wind speed at the gradient height under terrain D is 46.2 m/s.

AMD is considered as the actuator, installed on the top of the building, which weighs 423 T, about 1% of the first modal mass of the JIN MAO Building. The first two modal acceleration responses at the top of the buildings are to be controlled.

In order to evaluate the robustness of the controller, the uncertainty of the building stiffness is considered since the active controllers are not sensitive to the uncertainty in damping. The mode shapes are assumed unchanged. Stiffness uncertainties in seven cases from 15% to –15% are obtained by multiplying the first three modal frequencies 1.0724, 1.0488, 1.0247, 1.0000, 0.9747, 0.9487 and 0.9220, respectively. The controller is designed below and the same controller is applied to all the seven cases:

Control updating rate: $f = 75\,\text{Hz}$

Reference signal: $Sinusoidal = \sin(2\pi \times 16.148 \times n/f)$, n is time index

Forgetting factor: $\lambda = 0.1$

Identified model: $[h_1, h_2] = [8.60 \times 10^{-8},\ -1.34 \times 10^{-10}]$

Initialization for $n = 0$: $[w_1, w_2] = [0.0, 0.0]$, $\mathbf{C}_{NN}(n) = \begin{bmatrix} 1.0 \times 10^{12} & 0.0 \\ 0.0 & 1.0 \times 10^{12} \end{bmatrix}$

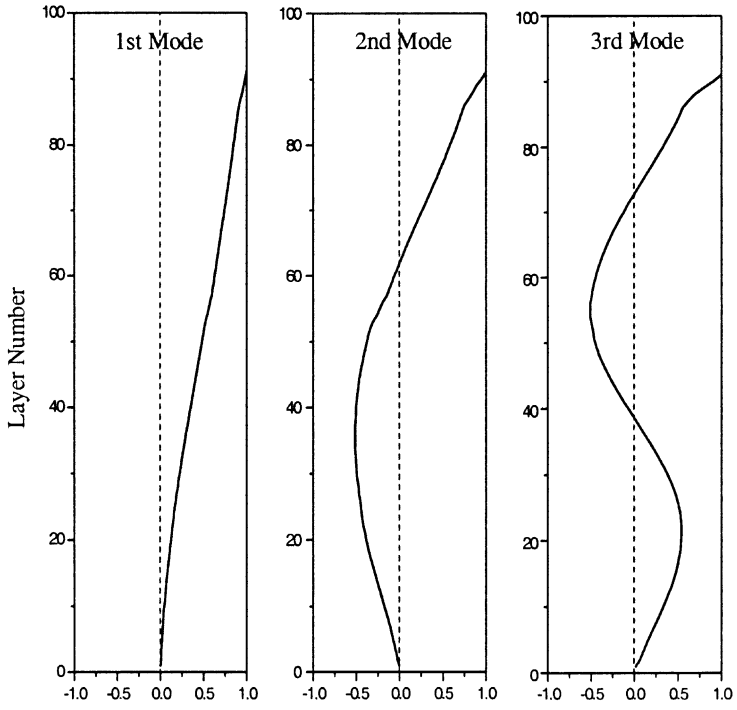

Fig. 5. First three mode shapes of JIN MAO Building.

Table 1
Modal parameters of JIN MAO building

Modal parameters	First mode	Second mode	Third mode
Modal frequency (Hz)	0.16148	0.66363	1.43068
Modal mass (T)	42323.089	33452.830	31114.356
Modal damping ration (%)	0.15	0.15	0.15

Fig. 6 shows time histories of uncontrolled and controlled accelerations of the zero-uncertainty building. The corresponding frequency spectra are shown in Fig. 7. The corresponding frequency spectra of the controller parameters and control force are presented in Fig. 8. Control efficiencies in peak and r.m.s. values in all seven cases are shown in Tables 2 and 3.

Fig. 6 indicates that the amplitude of the acceleration response is remarkably reduced. Comparing the frequency spectra of the uncontrolled and controlled accelerations shown in Fig. 7, one can see that the first two modal responses are reduced effectively. Fig. 8(a) shows that the controller parameters contain four dominant frequency components. Two of them are corresponding to the addition of the reference signal frequency and the first two modal frequencies, and the other two are corresponding to the subtraction of the reference signal

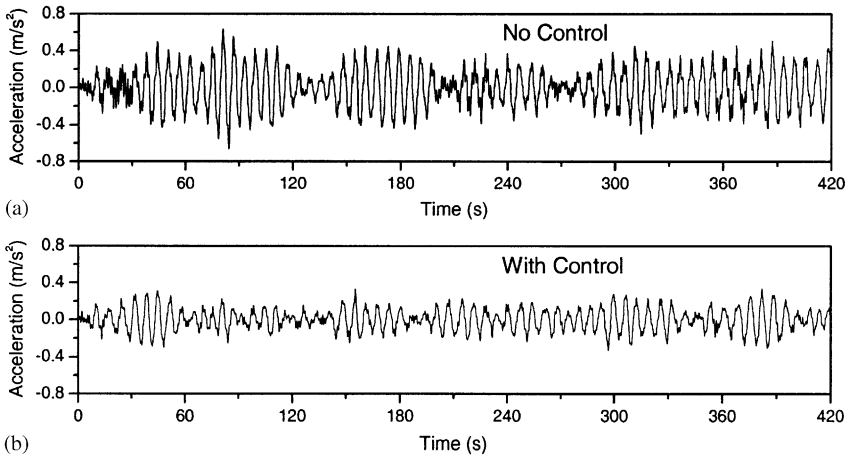

Fig. 6. Time histories of uncontrolled and controlled response of zero-uncertainty building.

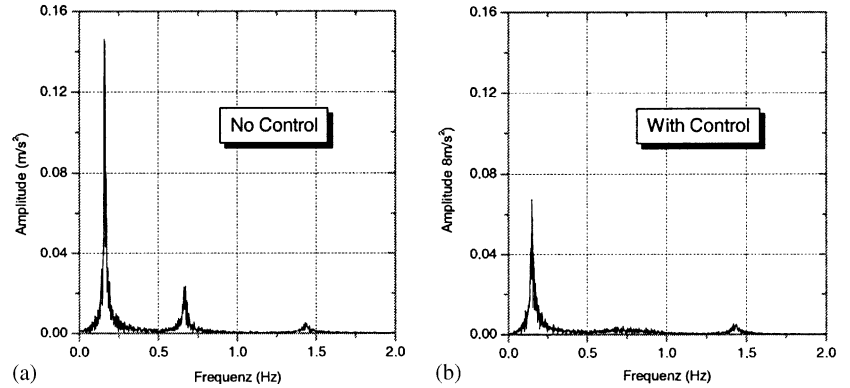

Fig. 7. Frequency spectra of uncontrolled and controlled response of zero-uncertainty building.

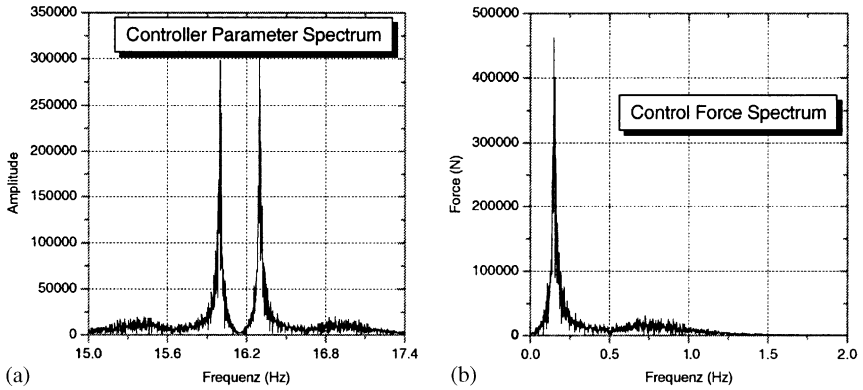

Fig. 8. Frequency spectra of the first controller parameter and control force for controlling zero-uncertainty building.

Table 2
Peak reduction efficiency under different stiffness uncertainty

Uncertainty (%)	No control (m/s^2)	With control (m/s^2)	Control efficiency (%)
15	56.735	35.524	37.386
10	61.318	34.114	44.365
5	65.381	35.510	45.687
0	66.527	34.749	47.767
−5	66.306	35.267	46.812
−10	68.097	36.849	45.888
−15	59.637	37.451	37.202

Table 3
r.m.s. Reduction efficiency under different stiffness uncertainty

Uncertainty (%)	No control (m/s^2)	With control (m/s^2)	Control efficiency (%)
15	20.987	11.737	44.075
10	21.819	11.722	46.276
5	23.096	11.711	49.294
0	22.182	11.829	46.673
−5	22.652	12.076	46.689
−10	23.186	12.310	46.908
−15	23.774	12.347	48.065

frequency and the first two modal frequencies. The control signal, which is the result of convolution of the reference sinusoidal signal and the controller parameters, consists of two dominant frequency components, corresponding to the first two dominant modal frequencies, shown in Fig. 8(b). The results in Tables 2 and 3 show that control efficiencies corresponding to different uncertainties do not change much, which demonstrates that the control system has good robustness.

It should be mentioned that the modal frequencies of the controlled structure are found to decrease slightly when the control system is running.

5. Designs of m.d.o.f. aeroelastic building model and AMD actuator

A m.d.o.f. aeroelastic model of a general super-tall building, which was designed and manufactured, is sketched in Fig. 9. It is of square cross-section with dimension of $0.15\,m \times 0.15\,m$. It is 1.125 m in height and about 8 kg in weight. In order to study the along-wind and across-wind responses, respectively, avoiding the coupling of responses in the two directions, the bending stiffness in the vibration direction is designed to be much smaller than that

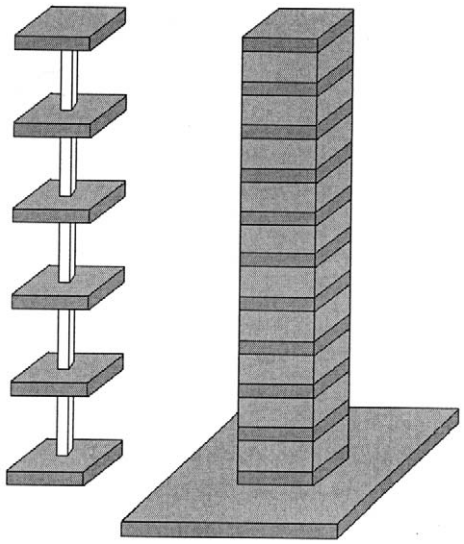

Fig. 9. Sketch of m.d.o.f. model of super-tall building.

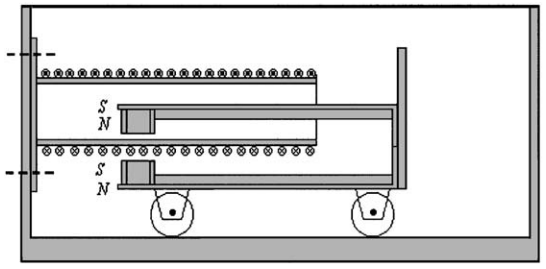

Fig. 10. Sketch of electro-magnetic AMD actuator.

in the other direction. The first four modal frequencies in the vibration direction are 2.2, 13.2, 33.5 and 62.8 Hz, respectively.

An AMD of an electro-magnetic type was designed and made, and is depicted in Fig. 10. The weight of the mass block is around 88 g, about 1.1% of the total weight of the designed super-tall building model. Its maximum stroke is limited to 2.0 cm. The maximum control force it can provide is about 0.3 N.

6. Wind field simulation and experimental setup

Wind tunnel tests were carried out in the TJ-1 boundary layer wind tunnel of Tongji University. Its working section is of 1.8 m in width and 1.8 m in height. The wind field simulation in the wind tunnel is achieved by a combination of turbulence generating spires, a barrier at the entrance of

the wind tunnel and roughness elements along the wind tunnel floor upstream of the model. Fig. 11 shows the simulated average wind speed profile and turbulent intensity of terrain D.

The experimental setup is shown in Fig. 12. Four accelerometers, which are mounted on the building model at the heights of 0.48, 0.68, 0.9 and 1.1 m, respectively, are used for measuring the acceleration responses. In addition, one accelerometer is set on the mass block of the AMD to measure its acceleration. The control system implementation is based on a TMS320C30 Digital Signal Processor, HY-8027A A/D-D/A board and a Personal computer. The AMD is installed on

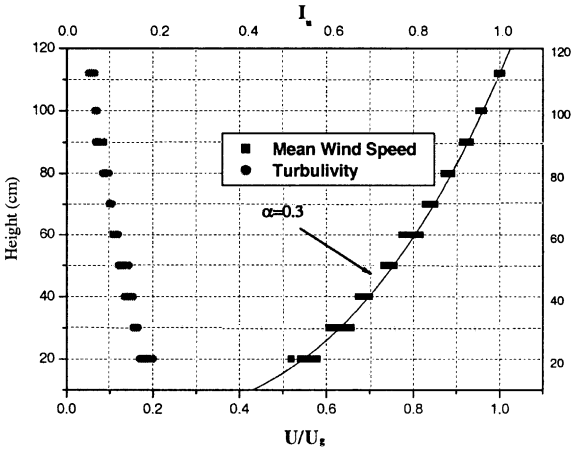

Fig. 11. Simulated wind field in wind tunnel.

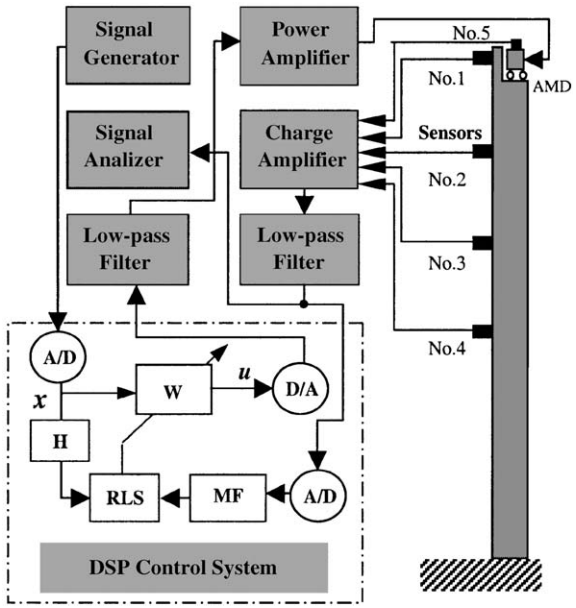

Fig. 12. Sketch of experimental setup.

the top of the building model. In order to reduce the friction damping, the mass block of the AMD is hung from the roof of the wind tunnel with four long threads when conducting the tests.

7. Experimental results and discussions

The objective of the tests is to experimentally investigate the efficiency and robustness of the present strategy for controlling the first modal response of super-tall buildings under wind actions, both in along-wind and across-wind directions. First four modal filters are computed before conducting the tests, which are presented in Table 4.

In order to evaluate the robustness of the control algorithm, the along-wind response control tests are conducted under eight different FIR models. The parameters of the test are: the wind speed is 4 m/s; the frequency of the reference signal is 200 Hz; the forgetting factor is set as 0.2; and the control updating rate is 12,000 Hz. Some time histories of the response with/without control and their frequency spectra of the building model are shown in Figs. 13 and 14, and the corresponding r.m.s. responses and efficiencies are listed in Table 5.

The across-wind response control test is conducted in a uniform wind field also under eight different FIR models. The test wind speed is 2.8 m/s. The frequency of the reference signal is selected as 200 Hz. The forgetting factor is set as 0.2. The control updating rate is 12,000 Hz. Some time history responses and their frequency spectrums are shown in Figs. 15 and 16. The corresponding r.m.s. responses and efficiencies are presented in Table 6.

From the results shown in Figs. 13 and 14 and Table 5, one can find that both peak and r.m.s. values of the along-wind response are effectively reduced. The results in Table 5 indicate that an

Table 4
First four modal filters of building model

First mode	Second mode	Third mode	Fourth mode
0.170	0.743	0.172	0.273
0.369	−0.072	0.006	−0.870
0.068	0.214	−1.200	1.069
0.390	0.886	1.022	−0.472

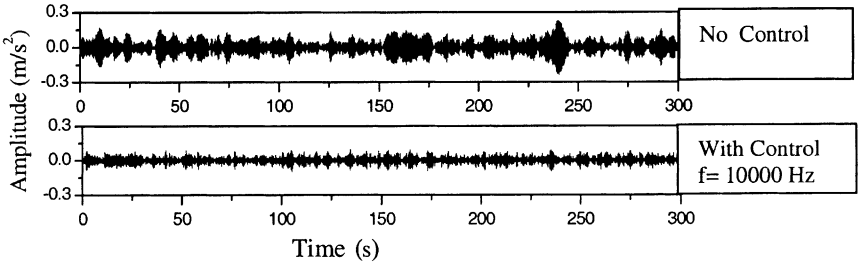

Fig. 13. Time histories of along-wind responses of Case 1 (uncontrolled response and controlled response with FIR Model [1.2, −0.05]).

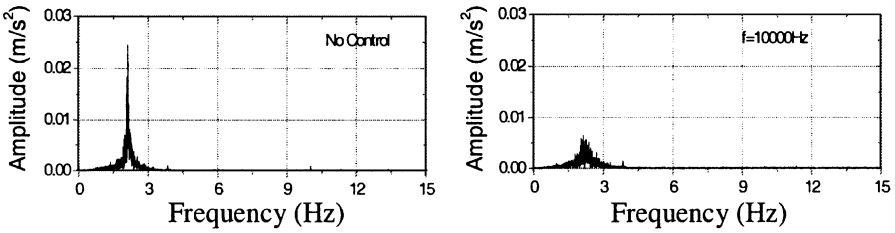

Fig. 14. Frequency spectrums of along-wind responses of Case 1 (uncontrolled response and controlled response with FIR Model [1.2, −0.05]).

Table 5
Control efficiencies of along-wind responses under different FIR models

FIR model (kg)	r.m.s. Response (m/s^2)	Efficiency
[0.4, −0.05]	0.0221	60.25
[0.8, −0.05]	0.0262	52.88
[1.2, −0.05]	0.0298	46.40
[1.6, −0.05]	0.0322	42.09
[2.0, −0.05]	0.0332	40.29
[2.4, −0.05]	0.0389	30.04
[2.8, −0.05]	0.0399	28.24
[3.2, −0.05]	0.0458	17.63
No control	0.0556	—

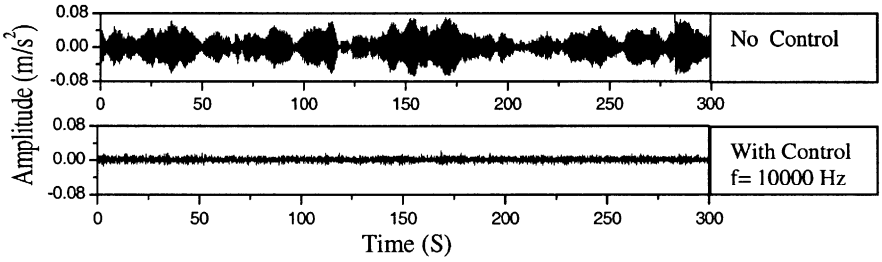

Fig. 15. Time histories of across-wind responses of Case 2 (uncontrolled response and controlled response with FIR Model [1.2, −0.005]).

SRS-based control system can run in stable state under quite different FIR models, and at the same time remarkable response reduction can be obtained. That demonstrates that the controls system is very robust. The characteristics of the results of controlling across-wind responses, presented in Figs. 15 and 16 and Table 6, are similar to those of controlling along-wind responses. The results also show remarkable control efficiency and satisfied robustness for across-wind-induced vibration of super-tall buildings. Moreover, due to the narrowband property of the

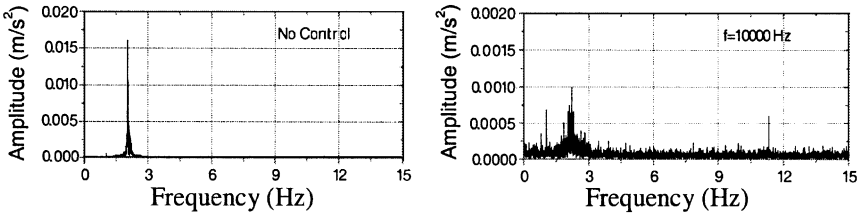

Fig. 16. Frequency spectrums of across-wind responses of Case 2 (uncontrolled response and controlled response with FIR Model [1.2, −0.005]).

Table 6
Control efficiencies of across-wind responses under different FIR models

FIR model (kg)	r.m.s. Response (m/s^2)	Efficiency (%)
[0.4, −0.005)]	4.66×10^{-3}	80.58
[0.8, −0.005]	6.83×10^{-3}	71.54
[1.2, −0.005]	8.40×10^{-3}	65.00
[1.6, −0.005]	1.03×10^{-2}	57.08
[2.0, −0.005]	1.14×10^{-2}	52.50
[2.4, −0.005]	1.15×10^{-2}	52.08
[2.8, −0.005]	1.16×10^{-2}	51.67
[3.2, −0.005]	1.25×10^{-2}	47.92
No control	2.40×10^{-2}	—

across-wind response, the efficiency of controlling across-wind vibration is seen to be higher than that of controlling along-wind response.

8. Concluding remarks

A Sinusoidal Reference Strategy is developed in this paper for adaptive feedforward vibration control of flexible structures. Numerical simulations and model studies are carried out for reducing wind-induced vibration of super-tall buildings. The results indicate that the present strategy has some superior properties in the construction of a reference signal, the reduction of the orders of the FIR model and the controller, less computation time and robustness, etc. Both the numerical simulations and experimental results further show remarkable control efficiencies and good robustness of the present strategy.

Acknowledgements

The authors gratefully acknowledge support from the National Science Foundation for Outstanding Youth, Foundation for University Key Teacher by the Ministry of Education, and National Natural Science Foundation (59895410).

This work is also partially supported by the Alexander von Humboldt Foundation and the Chinese National Post-doctor Foundation, which are also gratefully acknowledged.

References

[1] G.W. Housner, L.A. Bergman, T. Caughey, A. Chassiakos, R. Claus, S. Masri, R. Skelton, T. Soong, B. Spencer, J. Yao, Structural control: past present and future, Journal of Engineering Mechanics 123 (9) (1997) 897–971.
[2] B.F. Spencer Jr., M.K. Sain, Controlling buildings: a new frontier in feedback, Control Systems 17 (1997) 19–35.
[3] J. Suhardjo, B.F. Spencer, A. Kareem, Frequency domain optimal control of wind-excited buildings, Journal of Engineering Mechanics 118 (1992) 2463–2481.
[4] S. Ankireddi, H.T.Y. Yang, Multiple objective LQG control of wind-excited buildings, Journal of Structural Engineering 123 (1997) 943–951.
[5] M.Q. Feng, W. Chai, Design of a mega-sub-controlled building system under stochastic wind loads, Probabilistic Engineering Mechanics 12 (1997) 149–162.
[6] J.C. Wu, J.N. Yang, W.E. Schmitendorf, Reduced-order H^{∞} and LQR control for wind-excited tall buildings, Engineering Structures 20 (1998) 222–236.
[7] J.N. Yang, J.C. Wu, B. Samali, A.K. Agrawal, A benchmark problem for response control of wind-excited tall buildings, Proceedings of the Second World Conference on Structural Control (2WCSC), Kyoto, Japan, 1998, pp. 1407–1416.
[8] B. Widrow, S.D. Stearns, Adaptive Signal Processing, Prentice-Hall, Englewood Cliffs, NJ, 1985.
[9] B. Widrow Jr, J.R. Glover, J.M. McCool, J. Kaunitz, C.S. Williams, R.H. Hearn, J.R. Zeidler Jr, E. Dong, R.C. Goodlin, Adaptive noise control cancelling: principle and applications, Proceedings of the IEEE 63 (12) (1975) 1692–1716.
[10] G. Warnaka, Active attenuation of noise: the state of the art, Noise Control Engineering Journal 18 (3) (1982) 100–110.
[11] C.R. Fuller, Active control of sound transmission/radiation from elastic plates by vibration inputs: I analysis, Journal of Sound and Vibration 136 (1) (1990) 1–15.
[12] J.S. Vipperman, R.A. Burdisso, C.R. Fuller, Active control of broadband structural vibration using the adaptive LMS algorithm, Journal of Sound and Vibration 166 (2) (1993) 283–299.
[13] R.A. Burdisso, L.E. Suarez, C.R. Fuller, Feasibility study of adaptive control of structures under seismic excitation, Journal of Engineering Mechanics 120 (3) (1994) 580–592.
[14] K.G. Ma, X. Chen, et al., Adaptive control of wind-induced vibration of flexible structures: methods and experiments, Journal of Vibration Engineering 11 (2) (1998) 131–137 (in Chinese).
[15] S. Haykin, Adaptive Filter Theory, 3rd Edition, Prentice-Hall, Englewood Cliffs, NJ, 1996.
[16] P.S.R. Diniz, Adaptive Filtering: Algorithms and Practical Implementations, Kluwer Academic, Dordrecht, 1997.
[17] J.R. Treichler, C.R. Johnson, M.G. Larimore, Theory and Design of Adaptive Filters, Prentice-Hall, Englewood Cliffs, NJ, 2001.